Chemical Engineering Journal 383 (2020) 123157

Contents lists available at ScienceDirect

Chemical Engineering Journal

journal homepage: www.elsevier.com/locate/cej

Electrochemical nitrate reduction as affected by the crystal morphology and facet of copper nanoparticles supported on nickel foam electrodes (Cu/Ni)

Yu-Jen Shih[a,*], Zhi-Lun Wu[a], Yao-Hui Huang[b], Chin-Pao Huang[c]

[a] Institute of Environmental Engineering, National Sun Yat-sen University, Kaohsiung 804, Taiwan
[b] Department of Chemical Engineering, National Cheng-Kung University, Tainan 701, Taiwan
[c] Department of Civil and Environmental Engineering, University of Delaware, Newark, DE 19716, USA

HIGHLIGHTS

- Cu/Ni electrodes were successfully prepared using electrodeless method.
- Depositing time affected the morphology and crystal facet distribution of Cu.
- The Cu{1 1 1} facet played a significant role on nitrate reduction.
- Nitrogen selectivity was 55.6% at > −0.6 V vs. Hg/HgO.
- Complete nitrate reduction occurred at < −0.6 V vs. Hg/HgO.

GRAPHICAL ABSTRACT

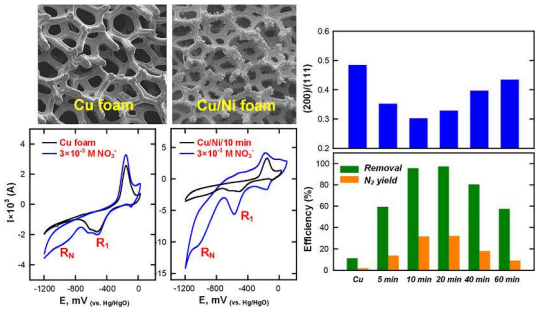

ARTICLE INFO

Keywords:
Electrodeless plating
Crystal facet
Nitrate
Selectivity
Electrode potential

ABSTRACT

Cu/Ni composite electrodes were prepared and studied for the electrochemical reduction of nitrate in aqueous solutions. Electrodeless plating technique, with tartrate as chelatant and formaldehyde as reducing agent, enabled the *in-situ* incorporation of Cu nanoparticles into the open-pore structured Ni foam to form Cu-Ni composite electrodes. X-ray diffractometer (XRD) and scanning electron microscopy (SEM) revealed that the crystal facet and grain morphology of Cu nanoparticles was closely controlled by the plating time and played a significant role in nitrate reduction and nitrogen selectivity. Cyclic voltammetry provided information on the electron transfer between surface nitrogen species and Cu/Ni electrodes. Electrochemical nitrate reduction was initiated at the onset potential of Cu(0)/Cu(I) redox reaction over a potential window of −0.6 V to −1.2 V. The preferential Cu{1 1 1} facet orientation improved the electron transfer process. Batch kinetics studies at constant current and potential showed that specific adsorption of nitrate and nitrite on the Cu{1 1 1} facet was critical to efficient electrochemical nitrate reduction. Moreover, the conversion of nitrogenous byproduct was potential-dependent. Results showed that N_2 selectivity was high (55.6%) at low overpotential (i.e., ⩾ −0.6 V vs. Hg/HgO. At high overpotential (i.e, < −0.6 V) there was complete of NO_3^- reduction with NH_4^+ as major byproduct.

1. Introduction

Nitrate is detrimental to the aquatic ecosystem. It is mostly originated from the nitrification step in the nitrogen cycle [1]. The intensive use of fertilizers in agriculture and uncontrolled wastewater discharges from various industries are primary contributors of nitrate to water resources, namely ground waters, rivers, and lakes [2]. Nitrate is a micro-nutrient that causes eutrophication in water bodies [3]. In

* Corresponding author.
E-mail address: yjshih@mail.nsysu.edu.tw (Y.-J. Shih).

https://doi.org/10.1016/j.cej.2019.123157
Received 23 July 2019; Received in revised form 21 September 2019; Accepted 12 October 2019
Available online 14 October 2019
1385-8947/

addition, ingesting nitrate from drinking water is harmful to human health such as methemoglobinemia, liver damage, and cancer [4], which has prompted the World Health Organization to impose a maximum nitrate concentration of 11.3 mg-N/L in drinking water [5]. Electrodialysis (ED), reverse osmosis (RO) and ion exchange (IE) are among the acceptable methods for the removal of nitrate from wastewater; however, disadvantages such as membrane fouling and high strength regenerants used in ion exchange regeneration limit the application of the above methods [6]. Biological denitrification such as autotrophic and heterotrophic processes require relatively large land space and long process time compared to chemical methods [7].

Catalytic hydrogenation technology, using hydrogen as electron donor, enables nitrate reduction over noble metallic (Pd, Pt) and transition metallic (Cu, Sn, In) catalysts are promising for nitrate removal [8,9]. Electrochemical engineering processes are emerging alternatives for nitrate removal owing to high effectiveness, low sludge production and remarkable environmental compatibility [10]. Recently, there have intensive interests in increasing nitrate removal and N_2 selectivity using various electrochemical catalytic systems [11,12]. Yao et al. studied indirect electrochemical nitrate reduction over zero-valent titanium anode and reported 83.4 and 78.5%, nitrate removal and N_2 selectivity, respectively [11]. Duan et al., demonstrated that a N-doped graphite carbon-encapsulated iron nanoparticles, Fe(20%)@N-C, exhibited 100% N_2 selectivity in the presence of NaCl [12]. Cu, known to promote electron transfer, is more reactive toward nitrogen than other metals [13]. Factors such as particle size, shape, morphology, and crystal facet, dependent on process and operation conditions, determine the catalytic reactivity and selectivity [14]. We have previously reported that ammonia can be removed through anodic oxidation over metal oxides, such as PbO_2 and NiOOH, but slow nitrate reduction together with the low cathodic current efficiency that led to low selectivity toward nitrogen gas remained a future technology challenge [15,16]. Hence, an effective electrode capable of reducing nitrate simultaneously during the anodic oxidation of ammonia is needed as to increase nitrogen selectivity.

The effect of morphology of Cu nanoparticles on electrochemical nitrate reduction is scarcely studied. It is hypothesized that the morphology (shape and size) and the crystal facet of Cu nanoparticles can affect the mode and kinetics of electrochemical nitrate reduction. Metallic copper was electrodeless deposited onto the nickel foam using tartrate (H_2T) as chelating agent and formaldehyde as electron donor [17,18] according to the following chemical reactions:

$$Cu^{2+} + 2OH^- + 2T^{2-} = CuT_2(OH)_2^{4-};\ K = 10^{20.7} \quad (1)$$

$$CuT_2(OH)_2^{4-} + 2HCHO + 2OH^- = Cu^0 + 2HCOO^- + 2T^{2-} + 2H_2O + H_2;\ K = 10^{19.87} \quad (2)$$

Voltammetry was used to study the electron transfer between the redox couple of Cu^0/Cu(I) and NO_3^-/N_2. Cu nanomaterials were characterized by X-ray diffractometer (XRD), scanning electron microscope (SEM), and X-ray photoelectron spectrometer (XPS). Overall it was to assess the effect of crystal facet and morphology of Cu nanoparticles on the mode and efficiency of nitrate reduction.

2. Materials and methods

2.1. Electrodeless deposition of Cu over Ni foam substrate

All reagents were of analytical grade and used without purification. The electrodeless plating of Cu was conducted on Ni foam (sheet thickness = 2 mm, area density ~250 g/m^2, mesh number = 94 ± 10), purchased from Innovation Materials Co., Ltd., Taiwan. The Ni foam was initially sensitized with 0.1 M $SnCl_2$ (Snowa Chemicals Inc. Mueche Khort, Isfahanm, Iran) and 0.1 M HCl, followed by activation with 5×10^{-3} M $PdCl_2$ (Sigma-Aldrich Co. St. Lewis, MO USA) and 0.25 M HCl. The plating bath was prepared in 0.05 M of $CuSO_4$ (Honeywell Fluka™, Morris Plains, NJ, USA) with 0.15 M of sodium tartrate (Alfa Aesar, Ward Hill, MA, USA) as chelating agent. The solution pH was adjusted to 12.5 using NaOH (Nihon Shiyaku Industries, Kyoto, Japan) when the color of the mixture gradually turned from light blue to indigo. The activated Ni foam was immediately dipped into the bath, and a specific amount of formaldehyde solution (Nihon Shiyaku Industries, Kyoto, Japan) was added dropwise. Note that hydrogen bubbles evolved from the electrode surface during Cu deposition. The Cu/Ni electrodes, designated according to the electrodeless plating time, for example, Cu/Ni/5-min and Cu/Ni/−90 min for 5 and 90 min, respectively. Then the electrodes were rinsed with 0.1 M HCl, washed with deionized water, and dried in vacuum before use.

2.2. Electrochemical analysis

Electrochemical experiments were carried out with a potentiostat (CHI611C, CH Instruments, Inc., Austin, TX, USA), in which Cu/Ni electrodes, prepared at various deposition times, were applied as working electrodes. The counter electrode was iridium oxide-coated titanium (Ti/IrO_2) and the reference electrode was Hg/HgO/1M NaOH (E^0 = 0.14 V vs. NHE) (RE-61AP, ALS Co. Ltd., Tokyo, JAPAN). The stock ammonium solution was prepared with ammonium sulfate, $(NH_4)_2SO_4$, (J.T. Baker, Phillipsburg, NJ USA). Sodium sulfate (Na_2SO_4, Sigma-Aldrich Co., St. Lewis, MO, USA) was the supporting electrolyte. The solution pH was adjusted to a specific value with sodium hydroxide (NaOH, Merck KGaA, Darmstadt, Germany) and sulfuric acid (H_2SO_4, 95%, Sigma-Aldrich Co., St. Lewis, USA).

2.3. Batch electrochemical reduction of nitrate

Batch electrochemical reduction of nitrate experiments were conducted in constant current mode. The Cu/Ni composite was rolled into rod with a diameter of 3.5 cm and length of 7.5 cm (total effective area ~80 cm^2) as working electrode. A Ti/IrO_2 cylinder of 5 cm in diameter, surrounding the Cu/Ni electrode, was the counter electrode. A commercial Cu foam (sheet thickness = 2 mm, mesh number = 100 openings per linear inch) was used as a controlled electrode for comparison with Cu/Ni electrodes. The nitrate removal efficiency (R, %) and nitrogen species conversion (S_N, %) were calculated at specific reaction time, *t*, according to the following equations:

$$R(\%) = \frac{C_{NO_3^-,0} - C_{NO_3^-,t}}{C_{NO_3^-,0}} \times 100 \quad (3)$$

$$S_N(\%) = \frac{C_N}{C_{NO_3^-,0} - C_{NO_3^-,t}} \times 100 \quad (4)$$

where C_N stands for the concentration of nitrogen product, such as NH_4^+-N, NO_2^--N, and N_2-N in mol/L, respectively.

2.4. Chemical analysis

A flow injection analyzer (FIA, Lachat's Quik Chem 8500 Series 2, Loveland, Colorado, USA) was used to analyze the concentration of aqueous nitrogen species (NO_3^--N, NH_4^+-N, NO_2^--N). Nitrate was reduced to nitrite (in a copperized cadmium column) prior to diazotization of nitrite with sulfanilamide ($H_2NC_6H_4SO_2NH_2$, Sigma-Aldrich Co., St Lewis, MO, USA) followed by coupling with N-(1-naphthyl)-ethylenediamine dihydrochloride (NED, $C_{10}H_7NHCH_2CH_2NH_2{\cdot}2HCl$, Sigma-Aldrich Co., St. Lewis, MO, USA) to obtain the concentration of total oxidized nitrogen (NO_x). The quantity of pink azo dye produced was then calibrated spectrophotometrically at 540 nm [19]. Nitrate concentration was the difference between NO_x and nitrite, which was determined separately. Measurement of ammonia was based on the indophenol method (at 630 nm) according to the Berthelot reaction, which involved reaction among phenoxide ($NaOC_6H_5{\cdot}3H_2O$), hypochlorite (NaClO), and ammonia, with nitroprusside ($Na_2[Fe(CN)_5NO]$)

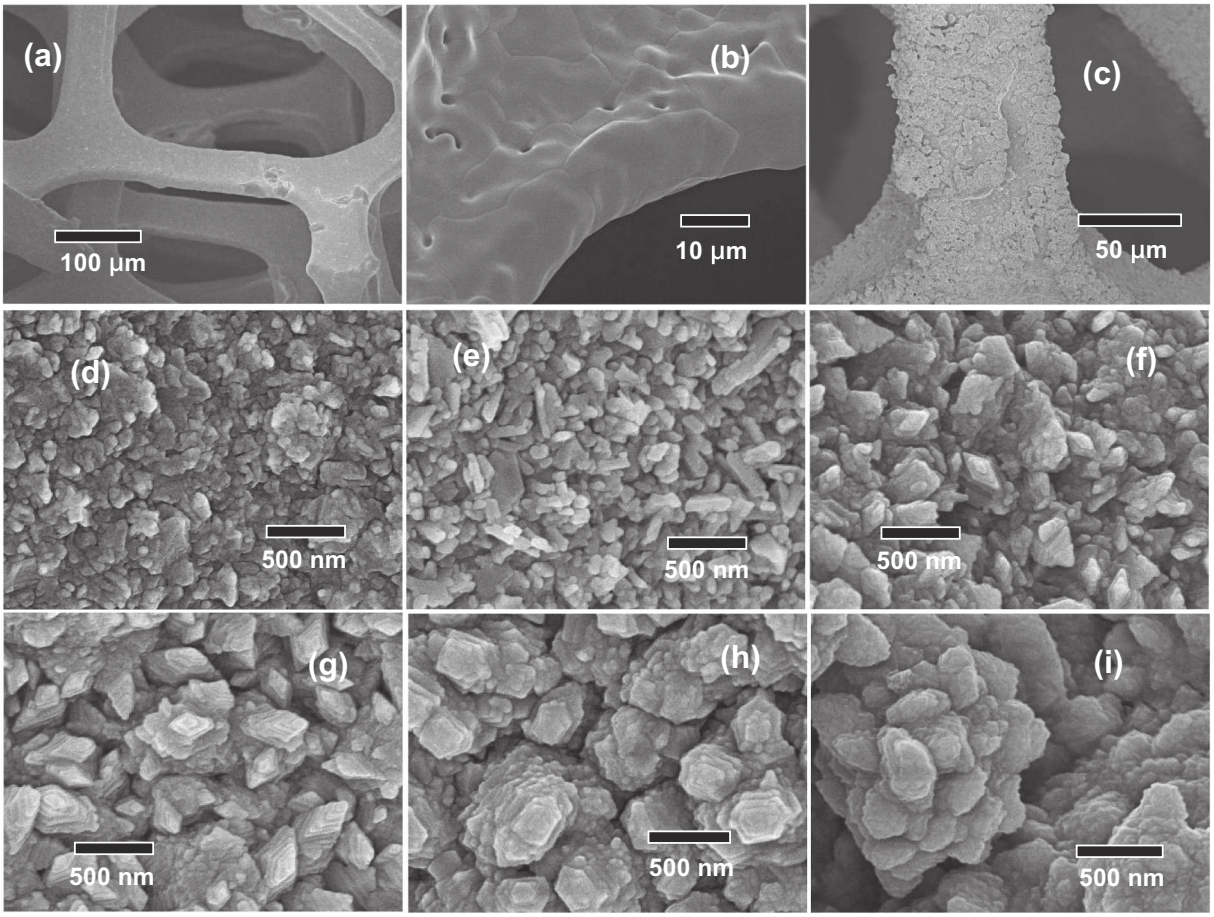

Fig. 1. SEM micromorphology of Ni foam at (a) 200×, (b) 2000×; (c) Cu/Ni electrode (600×) by electrodeless Cu plating at different duration: (d) 5 min, (e) 10 min, (f) 20 min, (g) 40 min, (h) 60 min, and (i) 90 min.

(Riedel-deHaën AG, Wunstorfer Straße, Seelze, Germany) as catalyst. The detection limit was 0.2 μg/L for NH_4^+-N, and 0.25 μg/L for both NO_2^--N and NO_3^--N. Deionized water used for the preparation of all solutions was purified with a laboratory-grade RO-ultrapure water system (resistivity > 18.18 MΩ cm).

The micro-morphology of the electrode surface was observed with scanning electron microscopy (SEM, JSM-6700F, JEOL Ltd., Japan). The crystallographic structure was analyzed by X-ray diffraction (XRD, DX III, Rigaku Co., Tokyo, Japan) operated with Cu Kαsource (λ = 1.5406 Å) at a scan rate of 0.06° s^{-1} in the incidence angle range of 20–85° (2θ). The chemical state of electrodes was characterized by X-ray photoelectron spectroscopy (XPS, PHI 5000 VersaProbe, Physical Electronics, Inc., USA) with a monochromatic Al Kα X-ray source (1487 eV).

3. Results and discussion

3.1. Characterization

Fig. 1 shows the micromorphology of Cu/Ni electrodes at different plating time observed under SEM. The Ni foam was composed of interconnected pores with skeletons at an average of 50 μm in diameter; the smooth surface of Ni metal was decorated with Cu crystals after plating (Fig. 1a–c). Under high magnification, the size of crystal clusters increased with increasing deposition time. The shape of single Cu crystals were granule, rod, rhombus, and hexagon (Fig. 1d–i). Obviously Cu particulates aggregated to polycrystalline with time. Fig. 2a shows the XRD pattern of Cu/Ni electrodes. The intensity of the two main peaks at 43.3° and 50.4°, referred to the planes of Cu{1 1 1} and Cu{2 0 0}, respectively, vividly increased with plating time. Fig. 2b shows that the mass of Cu increased from 2 to 12 wt% when the deposition time was increased from 5 to 90 min. Cu content of Cu/Ni electrodes was determined by electrode mass difference before and after Cu plating on a dry-weight basis. Note that the grain size did not change significantly and remained at an average diameter of 20 and 35 nm, estimated based on the Cu{1 1 1} and Cu{2 0 0} plane, respectively, according to the Scherer equation. The aggregation of primary grains oriented in different facet increased the particle size of the Cu crystals (shown under SEM). Fig. 2c gives the area ratio of Cu{2 0 0}/Cu{1 1 1} peak of Cu/Ni electrodes. The minimum Cu{2 0 0}/Cu{1 1 1} value was observed at around 10–20 min of plating time, which approached ultimately to that of the Cu foam, which implied initial crystal growth in the Cu{1 1 1} direction as to eliminate the surface energy of the Cu{1 1 1} plane. Crystal ripening involves the growth kinetics that may dimensionally transit from the facet of high surface energy to that of the lowest Gibbs energy [20]. Meanwhile, the effect of ripening is to alter the crystal size distribution with time in typical colloidal system in equilibrium with its saturated solution [21]. The Cu{1 0 0} facet is known to have a lower density of mobile holes than that of Cu{1 1 1} and Cu{1 1 0}, which explains the relatively low photocatalytic activity of Cu{1 0 0} in Cu_2O [22]. Thus, the plating time could be an important factor affecting the electron transfer of surface species. As shown in Fig. 3a, a significant portion of copper coated on the Ni substrate was in the Cu(II) state (934.3 eV) based on XPS spectra of Cu $2p_{3/2}$ orbitals, which declined and transformed to the Cu(0)/Cu(I) state (932.3 eV) [23] with increasing plating time. From the corresponding O 1s orbitals (Fig. 3b), Cu with the hydroxyl group (531 eV) predominated initially, and later evolved as an oxide film (530.7 eV) [24], which also indicated

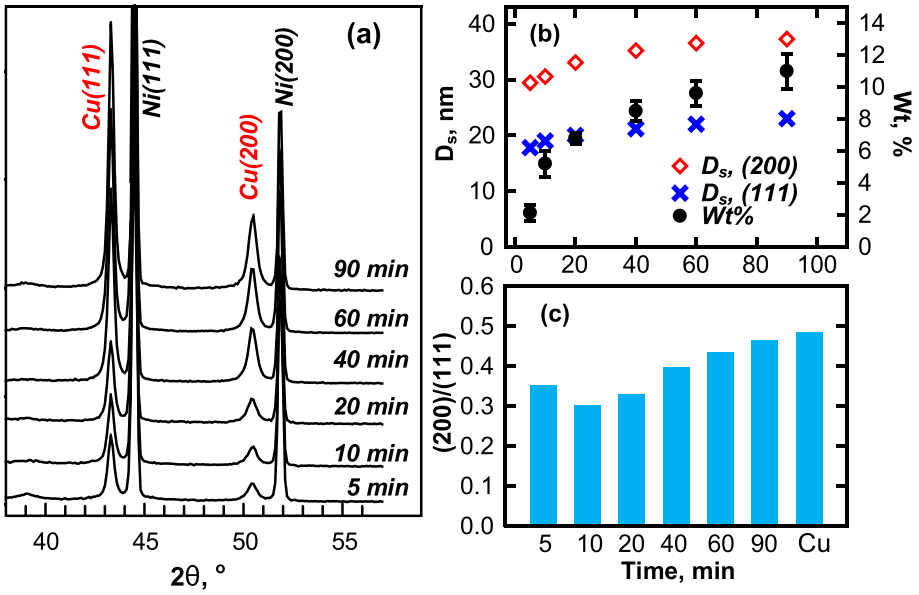

Fig. 2. (a) XRD analysis of Cu/Ni electrodes, and the corresponding (b) grain size and (c) area ratio of (2 0 0)/(1 1 1) plane.

the change in oxidation states of the Cu particles with time.

3.2. Electrochemical analysis

The characteristics of the electrochemical nitrate reduction over the Cu/Ni electrode were studied using cyclic voltammetry. Fig. 4a presents the current profile of Cu/Ni/10-min electrode in the presence of 0.1 M Na_2SO_4 supporting electrolyte scanned between varying upper limit potentials (from −0.7 V/−0.2 V to −0.7 V/+0.25 V vs. Hg/HgO). Results showed that the oxidative corrosion for $Cu^{(0)}$ on the Ni substrate had two peak potentials of O_1 and O_2 at −0.2 V and +0.05 V, respectively, which can be attributed to the formation of oxide films:

$$2Cu^{(0)} + H_2O \rightarrow Cu_2O(s) + 2H^+ + 2e^-(O_1) \quad (5)$$

$$Cu_2O(s) + H_2O \rightarrow 2CuO(s) + 2H^+ + 2e^-(O_2) \quad (6)$$

The sharp enhancement in current as scanning at upper limit of potential up to +0.1 V (O_3) suggested that the passivated oxide, protecting the metal surface, was totally oxidized to the Cu^{2+} state, i.e.,:

$$Cu^{(0)} \rightarrow Cu^{2+} + 2e^-(O_3) \quad (7)$$

As a result, the salt film that accumulated at the electrode surface was polarized with a potential-independent current density. To avoid the interference of electrode dissolution with nitrate redox reaction, the potential window of −1.2 V/+0 V, where Cu(0)/Cu(I) occurred, was studied.

As shown in Fig. 4b, the reversible peak current of Cu/Ni/10-min redox was a linear function with respect to the square root of the scan rate, which suggested that the electron transfer in Eq. (5) was limited by proton diffusion. The proton diffusion coefficient was 8.85×10^{-13} cm^2/s and 1.26×10^{-12} cm^2/s for the anodic and the cathodic reaction, respectively, (Fig. S1) which was comparable to that

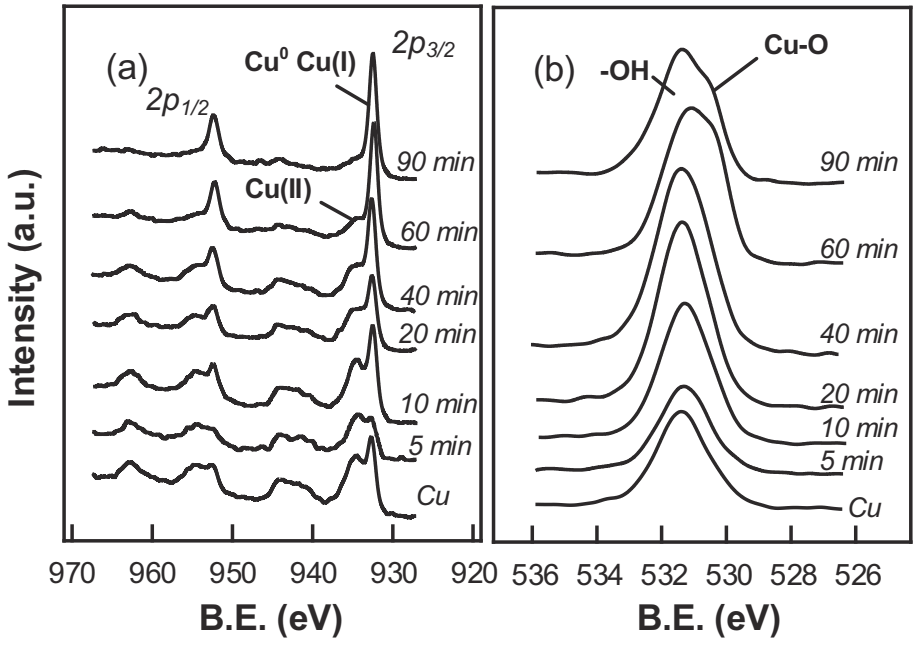

Fig. 3. XPS of Cu/Ni electrodes at the binding energy ranges of (a) Cu 2p and (b) O1s.

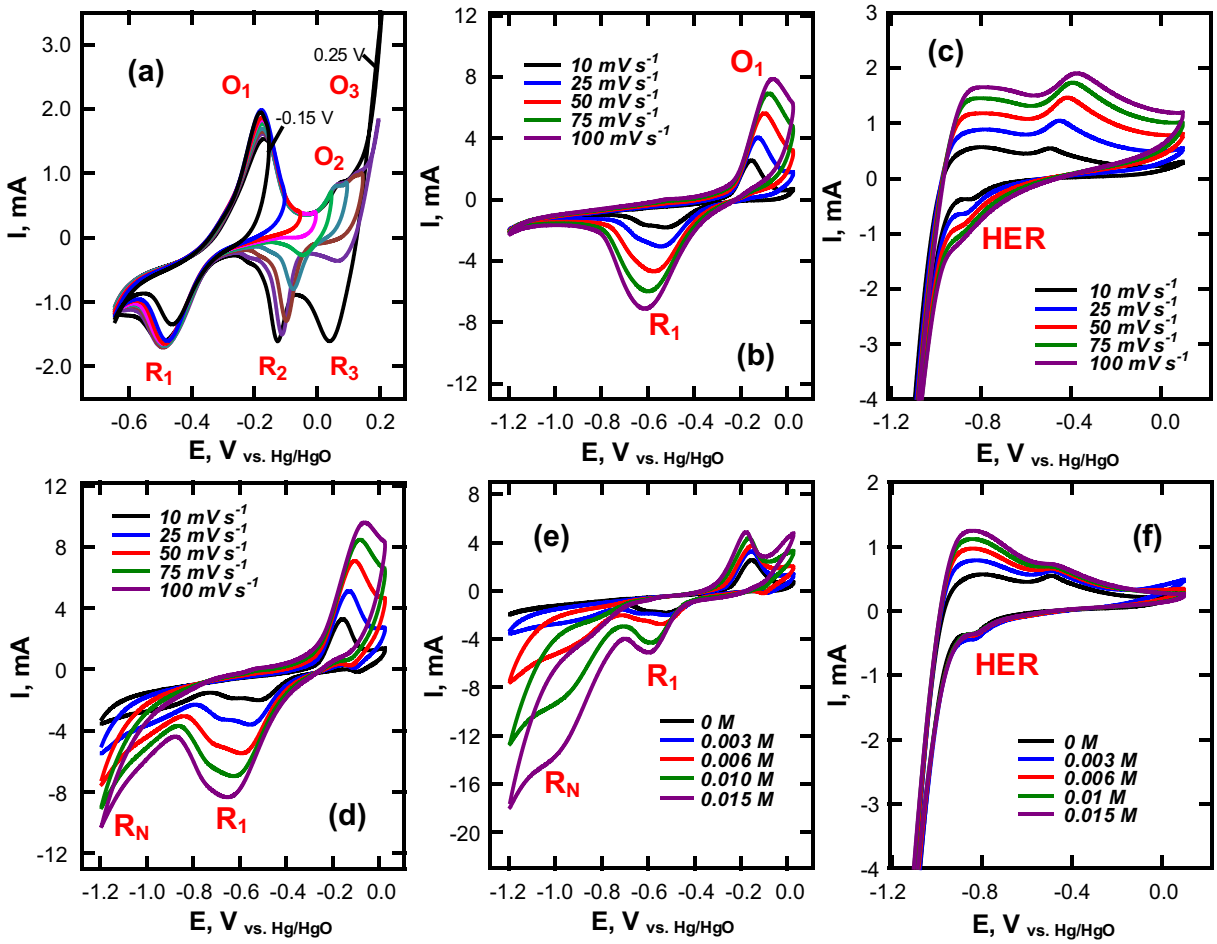

Fig. 4. Cyclic voltammetry of (a) Cu/Ni electrode scanned in the range of −0.7 V/ + 0.25 V in the presence of 0.1 M Na_2SO_4 (10 mV s^{-1}); (b) Cu/Ni/10-min and (c) Ni foam at different scan rate; Cu/Ni/10-min in nitrate solution under different (d) scan rates ([NO_3^-] = 3 × 10^{-3} M) and (e) different NO_3^- concentrations (10 mV s^{-1}); (f) Ni foam in different nitrate solutions.

of the Ni/NiOOH electrode [16,25]. In such potential range, the Ni foam substrate did not exhibit electrode redox reactions, but a strong reduction current for hydrogen evolution reaction (HER) (Fig. 4c). Note that the higher overpotential of gas evolution on Cu foam, in comparison with Ni foam, would benefit the reduction of target electrolyte over a Cu/Ni electrode. In nitrate solution, the current at R_1 improved and an additional current appeared at around −1.0 V (R_N, Fig. 4d), which was also diffusion-controlled. Furthermore, peak currents at R_1 and R_N, as a function of nitrate concentration shown in Fig. 4e, proved the nature of multistep electrode process involving the redox reaction of $Cu^{(0)}$ and NO_3^-. The current profile in Fig. 4f never changed with increasing nitrate concentration on the Ni foam substrate, which suggested that the metallic Ni was incapable of inducing nitrate redox reaction.

Fig. 5 shows the linear regression between peak currents at R_1 and R_N and nitrate concentration over Cu/Ni electrodes prepared at various plating times. Fig. S2 shows the voltammetry in the presence of NO_3^-. According to the Nicholson and Shain equation: $i_p = 2.99 \times 10^5 n\alpha^{1/2} A D^{1/2} C^* v^{1/2}$, the peak current ($i_p$) of a faradaic reaction is proportional to the concentration of electrolyte (C*, mol cm^{-3}) under fixed scan rate v (0.01 V s^{-1}), effective area A (3 cm^2), and diffusion coefficient D (1.4 × 10^{-5} cm^2 s^{-1}). If the electron number of redox reaction (n) is known, the slope in Fig. 5a and b should be a function of the transfer coefficient (α). One can assume that R_1 is the step of one electron transfer assigned to Cu(I) oxide reduction (the backward reaction of Eq. (5)), and then its increase in current with increase in nitrate concentration may be resulted from the indirect redox reaction between $Cu^{(0)}$ and the adsorbed NO_3^- species (Eqs. (8)–(10)) [26].

$$Cu^{(0)} + NO_3^- \rightleftharpoons Cu^{(0)}NO_3^- \quad (8)$$

$$Cu^{(0)}NO_3^- + 2H^+ \rightarrow Cu^{(+1)}NO_2 + H_2O \quad (9)$$

$$Cu^{(+1)}NO_2 + e^- \rightarrow Cu^{(0)}NO_2 \quad (10)$$

The catalytic effect of Cu/Ni electrode on steps (i.e., 8–10) may be similar to the incipient hydrous oxide-adatom mediator (IHOAM) model [27], which describes the activated chemisorption. The monolayer redox Cu(0)/Cu(I) couple on the electrode surface catalytically mediates the supplementary electron from the reactive species, i.e., NO_3^-. Increase in cathodic potential, further increased the reduction of the adsorbed species, i.e., nitric oxide. The strong polarization current at R_N, involved at least four electrons to yield one molecular nitrogen on the Cu surface [28,29], was the precursor of gaseous nitrogen and ammonia nitrogen.

$$Cu^{(0)}NO_2 + 4H^+ + 4e^- \rightarrow Cu^{(0)}N + 2H_2O \quad (11)$$

$$2Cu^{(0)}N \rightleftharpoons Cu_2^{(0)}N_2 \quad (12)$$

With n = 1 and = 4 for the limiting currents of R_1 and R_N, respectively, the transfer coefficients (α) were calculated according to the Nicholson and Shain as shown in Fig. 5c. A controlled sample (the commercial Cu foam) had α value of 0.27 and 0.55 for R_1 and R_N, respectively. By contrast, among electrodes prepared at different plating times, the Cu/Ni/20-min electrode had a maximal α value of around 0.8

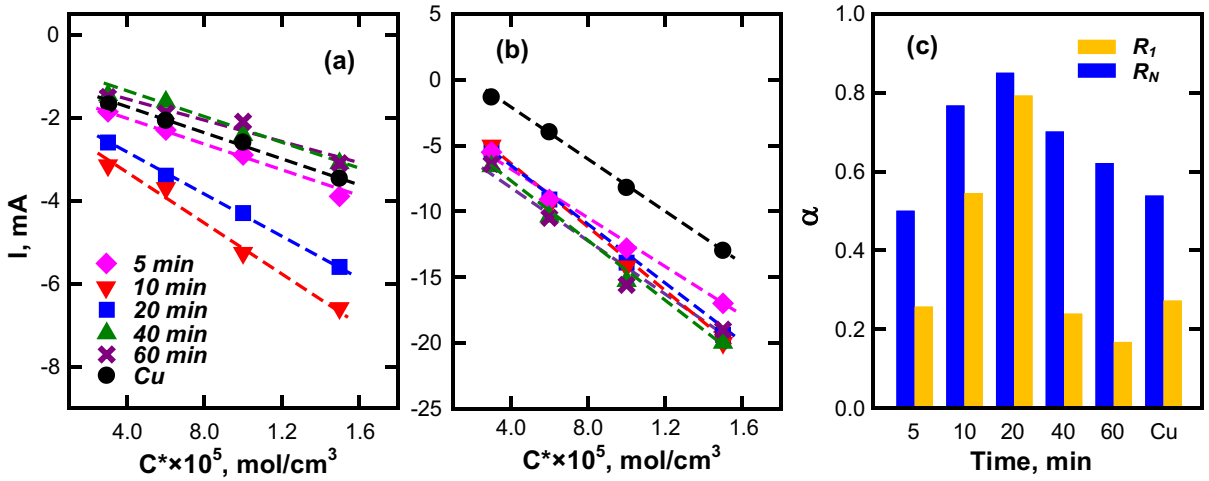

Fig. 5. Linear regression of peak current of (a) R_1 and (b) R_N versus nitrate concentration, and (c) transfer coefficient for Cu/Ni electrodes prepared at different deposition time (min).

for both R_1 and R_N steps.

Fig. 6a and 6b show the polarization (log *i*-*E*) of Cu/Ni electrodes in the presence of 0.1 M $NaClO_4$ (i.e., HER) and 5×10^{-2} M KNO_3 plus 0.1 M $NaClO_4$ supporting electrolyte, respectively. The formal potential of H_2 formation occurred at around −1.3 V on Cu foam, then increased to −1.0 V on Cu/Ni electrodes due to the low overpotential of Ni

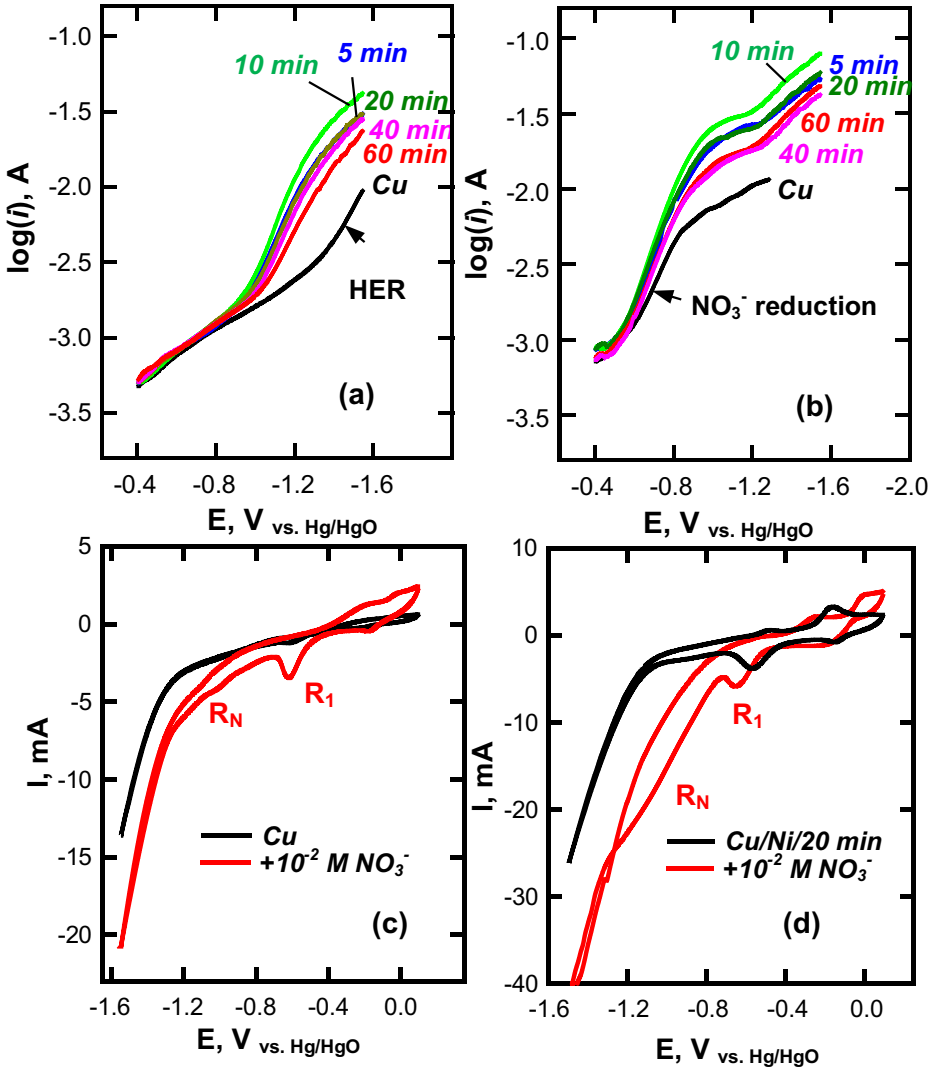

Fig. 6. log *i* vs. E plots for Cu/Ni electrodes (a) without and (b) with the presence of 5×10^{-2} M KNO_3. Comparison in the voltammetry of (c) Cu and (d) Cu/Ni/20-min electrodes.

Table 1
Slopes of log*i*-*E* for hydrogen evolution reaction (HER) and nitrate reduction on Cu and Cu/Ni electrodes.

	Tafel slope *b*, mV dec^{-1}	
Electrodes	HER	NO_3^- reduction
Cu	183	149
Cu/Ni/5-min	177	120
Cu/Ni/10-min	159	113
Cu/Ni/20-min	166	117
Cu/Ni/40-min	170	135
Cu/Ni/60-min	174	135

substrate in HER. Besides, note that the Tafel slope *b* is a function of α and *n* (electron number of the limiting step), according to the reduction polarization $b = (2.303RT)/(\alpha nF) = 59/\alpha n$ (mV dec^{-1} @ STP). As listed in Table 1, the Cu/Ni electrodes prepared at plating time of 10 and 20 min exhibited relatively small *b* value of about 160 mV dec^{-1}, compared to $b = 183$ mV dec^{-1} of pure Cu metallic electrode. The decline in *b* of HER with increase in Cu plating time implies that Ni has higher affinity toward H^+ than Cu, which could assist protonation of steps shown in Eqs. (9) and (11) [30]. On the other hand, the *b* value of NO_3^- was also increased with increasing the plating time, under which the ratio of Cu{2 0 0}/Cu{1 1 1} peak areas increased (Fig. 2c). The results of voltammetry and polarization curve suggested that the morphology of Cu particulates could be a critical factor affecting the performance of Cu/Ni electrodes in nitrate reduction toward nitrogen selectivity. Fig. 6c and 6d compare the CV for commercial Cu foam and Cu/Ni/20-min electrodes, respectively, without and with 10^{-2} M of KNO_3. The Cu particles formed during electrodeless plating (Cu/Ni) showed more pronounced R_1 peak (@ −0.6 V), were responsible for larger active surface and greater Cu(0)/Cu(I) transition, than pure Cu electrode. In the presence of KNO_3, the first electron step from the adsorbed nitrate (Eqs. (8)–(10)) by improving R_1 peak occurred on both electrodes, whereas much higher current of R_N was created on the Cu/Ni electrode compared to that on Cu electrode as more negative potentials were applied. That is, the pure Cu metal was less active in mediating the transfer of electrons in intermediates, or the steps of NO_3^- conversion would not be completed in the potential range of −0.6 and −1.2 V.

3.3. Constant current and constant potential

Fig. S3 shows the effectiveness of NO_3^- reduction as a function of time (initial NO_3^--N = 50 ppm, pH ~ 8.5, 0.1 M Na_2SO_4 as an inert electrolyte) over pure Cu and Cu/Ni electrodes prepared at various time intervals (i.e., 5–60 min). At a constant current of 3 mA cm^{-2}, the temporary concentration of the stable byproducts, namely, NH_4^+, and NO_2^-, are recorded. N_2, were calculated from mass-balance relationship. Some less stable gaseous nitrogen compounds, such as NO, N_2O, were possibly produced from catalytic NO_3^- reduction, while they could be rapidly transformed to N_2 and were not considered in the present work [3,31]. The electrochemical nitrate reduction rapidly proceeded over the Cu/Ni/10-min and Cu/Ni/20-min electrodes but was slow on the pure Cu metal and the Cu/Ni/60-min electrode. Such results agreed with those of voltammetry experiments, showing that a greater value of transfer coefficient (α) of nitrate reduction could be obtained by manipulating the facet oriented more toward Cu{1 1 1}. The removal efficiency of nitrate followed the order: Cu/Ni/20-min (97%) > Cu/Ni/10-min (95%) > Cu/Ni/60-min (57%) > Cu (11%) in 5 h of electrolytic reaction. Table 2 summaries the selectivity of nitrate conversion toward various nitrogenous compounds. Results show that S_N, in terms of N_2, was significantly related to the intensity of Cu {1 1 1} facet at different plating time, which improved from 17.5% over Cu to 33.1% over both the Cu/Ni/10-min and Cu/Ni/20-min electrode.

Table 2
Selectivity of nitrate conversion to nitrogenous byproduct over Ni foam, Cu foam, and Cu/Ni electrodes (current = 3 mA cm^{-2}, initial NO_3^--N = 50 ppm, 0.1 M Na_2SO_4).

	S_N, %			
	NO_2^--N	NH_4^+-N	N_2-N	R, %
Ni	21.6	60.5	18.0	2.4
Cu	0.1	82.5	17.5	11.3
Cu/Ni/5-min	6.4	70.3	23.2	59.4
Cu/Ni/10-min	0.5	66.4	33.1	95.7
Cu/Ni/20-min	0.3	66.6	33.1	97.2
Cu/Ni/40-min	1.0	76.5	22.5	80.4
Cu/Ni/60-min	0.8	83.2	16.0	57.4

In addition, the Ni foam, used as a substrate for Cu plating, exhibited a rather limited ability to mediate the electron transfer from nitrate according to voltammetry study, thus resulting in negligible nitrate removal (R = 2.4%).

According to Fig. 6c and 6d, the current created in the range of −0.6 to −1.2 V was ascribed to the presence of nitrate. Fig. S4 demonstrates the effect of constant potential (−0.6 V and −1.2 V vs. Hg/HgO) on the removal of nitrate and the evolution of nitrogen byproducts (initial NO_3^--N = 50 ppm, pH ~ 8.5, 0.1 M Na_2SO_4 as an inert electrolyte). Fig. 7 shows the effect of overpotential on the mode of

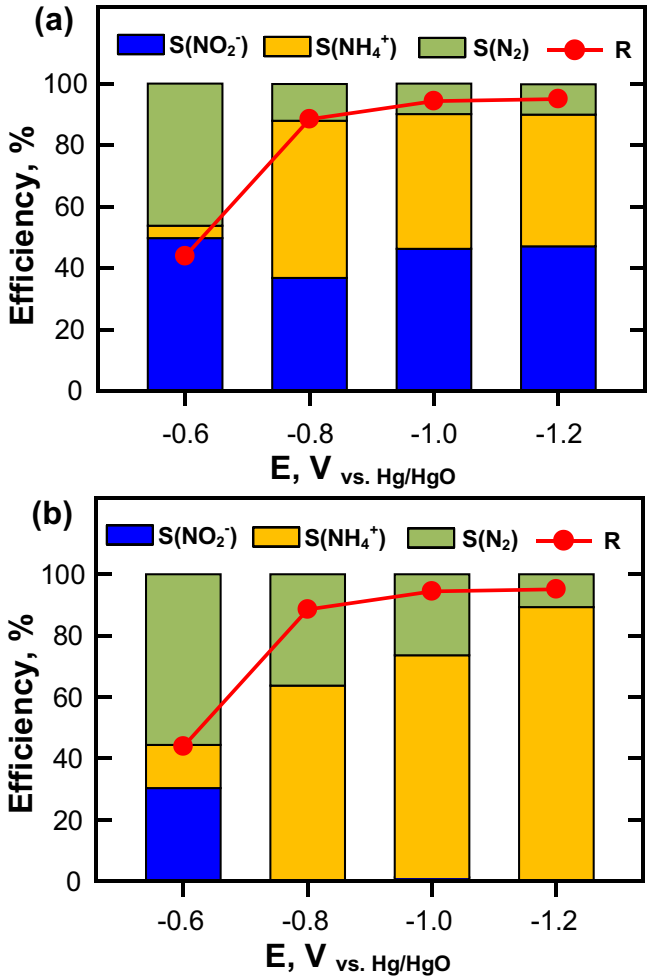

Fig. 7. Selectivity of nitrate conversion to nitrogenous byproduct on a) Cu foam and (b) Cu/Ni/20-min electrodes at different electrode potential (ref. electrode = Hg/HgO, counter electrode = Ti/IrO_2, initial NO_3^--N = 50 ppm, 0.1 M Na_2SO_4).

nitrate reduction over pure Cu and Cu/Ni/20-min electrodes. Generally, nitrate reduction increased with overpotential for both electrodes. At low electrode potential (−0.6 V), NO_3^- was preferentially converted to N_2 with S_N value of 46.3% and 55.6% over the Cu and the Cu/Ni/20-min electrodes, respectively (Table S1). However, with increasing electrode potential (to −1.2 V), the predominance of N_2 decreased, and the concentration of NH_4^+ became significant; at the end of electrolysis (4 h), the main byproducts over the Cu metal electrode were NO_2^- (47.1%) and NH_4^+ (42.9%) and those of Cu/Ni electrode were NH_4^+ (89.1%) and N_2 (10.7%). The heterogeneous catalysis may explain the difference in the selectivity of nitrogen conversion. Since detectable nitrogen compounds in the aqueous solution came from the desorption of surface species, the affinity between a specific crystal facet and chemicals that participated at the redox reactions (namely, NO_3^-, NO_2^-, NH_4^+, N_2, H^+) in the electrolyte would influence the sequence of reduction steps.

We visualize the following scheme as the overall mechanism of nitrate reduction on the Cu particulates (S2, Supplementary Information).

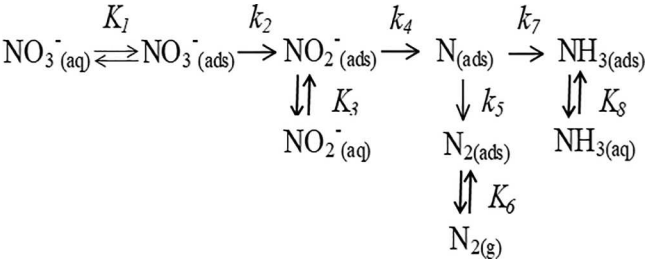

(13)

On the basis of voltammetric observation, total of 5 electrons throughout R_1 and R_N were transferred, which meant that the direct electrochemical reactions from NO_3^- to N (Eqs. (10) and (11)) accounted for the polarization current, and the production of NH_4^+-N resulted from the indirect protonation of nitrogen by the surface hydrogen as a strong reducing agent [32].

$$CuH^+ + e^- \rightarrow CuH\cdot \tag{14}$$

$$CuN + 3CuH\cdot \rightarrow CuNH_3 \tag{15}$$

By treating all surface adsorbed chemicals as steady-state species, including $\theta_{NO_3^-}$, $\theta_{NO_2^-}$, θ_N, θ_{N_2}, θ_{NH_3}, and θ_H, one has the following rate equations of NO_3^- and nitrogenous byproducts in the solution.

$$\frac{d[NO_3^-]}{dt} = -k_1^+\theta[NO_3^-] + k_1^-\theta_{NO_3^-} \tag{16}$$

$$\frac{d[NO_2^-]}{dt} = k_3^+\theta_{NO_2^-} - k_3^-\theta[NO_2^-] \tag{17}$$

$$\frac{d[N_2]}{dt} = k_6^+\theta_{N_2} - k_6^-\theta[N_2] \tag{18}$$

$$\frac{d[NH_4^+]}{dt} = k_8^+\theta_{NH_3} - k_8^-\theta[NH_4^+] \tag{19}$$

(S2. Supporting Information gives detail derivation of rate equations.)

The aqueous nitrogen species converted from an initial $[NO_3^-]_0$ were $[NO_2^-]$, $[N_2]$, and $[NH_4^+]$, and the total reduction rate was equal to the sum of NO_2^-, N_2, and NH_4^+ generation, namely,

$$[NO_3^-]_0 = [NO_3^-] + [NO_2^-] + 2[N_2] + [NH_4^+] \tag{20a}$$

and

$$-\frac{d[NO_3^-]}{dt} = \frac{d[NO_2^-]}{dt} + \frac{d[NH_4^+]}{dt} + \frac{1}{2}\frac{d[N_2]}{dt} \tag{20b}$$

Consequently, the concentration profile of nitrogen species in the solution as a function of time can be obtained by integrating Eq. (16) through Eq. (19).

Table 3
Rate constants and equilibrium constants of nitrate reduction over Cu and Cu/Ni electrodes at constant current of 3 mA cm^{-2}, and various electrode potentials (vs. Hg/HgO).

Electrodes	k_a ($\times10^{-3}$, min^{-1})	k_c ($\times10^{-2}$, min^{-1})	K_b	K_d($\times10^{-2}$)
Cu	1.0	20.0	0.80	35.0
Cu/Ni/5-min	5.0	2.1	0.5	9.5
Cu/Ni/10-min	10.0	9.0	0.40	9.0
Cu/Ni/20-min	14.0	4.0	0.23	10.0
Cu/Ni/40-min	6.0	1.2	0.75	11
Cu/Ni/60-min	3.5	20.0	0.70	4.0
	Commercial Cu foam			
vs. *Hg/HgO*	k_a ($\times10^{-3}$, min^{-1})	k_c ($\times10^{-2}$, min^{-1})	K_b	K_d($\times10^{-2}$)
−0.6 V	4.0	15.0	1.20	45.0
−0.85 V	21.0	5.5	1.10	18.0
−1.0 V	22.0	3.1	0.95	17.0
−1.2 V	24.0	2.8	0.77	5.0
	Cu/Ni/20 min			
vs. *Hg/HgO*	k_a ($\times10^{-3}$, min^{-1})	k_c ($\times10^{-2}$, min^{-1})	K_b	K_d($\times10^{-2}$)
−0.6 V	2.4	3.0	1.8	40.0
−0.85 V	21.0	6.0	1.6	19.0
−1.0 V	29.0	5.0	0.3	15.0
−1.2 V	25.0	3.0	0.2	5.5

$$[NO_3^-] = [NO_3^-]_0 e^{-k_a t} \tag{21}$$

$$[NO_2^-] = \frac{k_a K_b}{k_c - k_a}[NO_3^-]_0 (e^{-k_a t} - e^{-k_c t}) \tag{22}$$

$$[N_2] = \frac{2(k_c - k_a + k_a K_b)K_d}{k_c - k_a}[NO_3^-]_0 (1 - e^{-k_a t}) - \frac{2k_a K_b K_d}{k_c - k_a}[NO_3^-]_0 (1 - e^{-k_c t}) \tag{23}$$

$$[NH_4^+] = \frac{(k_c - k_a + k_a K_b)(1 - 2K_d)}{k_c - k_a}[NO_3^-]_0 (1 - e^{-k_a t}) - \frac{k_a K_b (1 - 2K_d)}{k_c - k_a}[NO_3^-]_0 (1 - e^{-k_c t}) \tag{24}$$

in which $k_a = \frac{k_1^+ k_2 \theta\theta_H [e]}{k_1^- + k_2\theta_H[e]}$, $K_b = \frac{k_3^+}{k_3^+ + k_4\theta_H[e]}$, $k_c = \frac{k_3^- k_4 \theta\theta_H[e]}{k_3^+ + k_4\theta_H[e]}$, and $K_d = \frac{k_5}{2k_5 + k_7\theta_H}$ are composite functions of rate constants in the reaction scheme, Eq. (13). The rate constant k_a is determined by the rate of adsorption (k_1^+) and 1st electron transfer (k_2) of NO_3^-; k_c is related to NO_2^- sorption (k_3^-) and surface N formation (k_4). The constant K_b describes the equilibrium of NO_2^- desorption (k_3^+) and N formation (k_4); K_d reflects the selectivity of N_2 (k_5) and NH_4^+ (k_7). Table 3 lists the rate constants and equilibrium constants of nitrate reduction over different electrodes under constant current and constant potential systems by fitting the data in Figs. S3 and S4 using Eqs. (21)–(24). Among the tested electrodes, Cu/Ni/20-min exhibited a relatively high k_a (1.4×10^{-2} min^{-1}) along with small K_b (0.23); that is, the Cu{1 1 1} plane may favor the adsorption of NO_3^- and NO_2^- anions, which leads to higher removal efficiency of NO_3^-. The predominance of Cu{1 1 1} on Cu/Ni/20-min electrode also improved the selectivity for N_2 according to its high K_d value. For cuprite structured (Cu_2O), each Cu has two oxygen neighbors; on the Cu{1 1 1} facet the dangling bonds of Cu can be positively charged, whereas the Cu{1 0 0} facet, fully saturated with oxygen bonds, has the lowest energy state [33,34]. Crystal facets of Cu{1 1 1} and Cu{1 1 0} should therefore interact with oxyanions more strongly than the electrically neutralized Cu{1 0 0} [35,36]. Under constant potential system, the Cu foam electrode had k_c value greater than k_a at studied potential to evolve the R_N current; which implied that the step for nitrate adsorption on the Cu/Ni foam was rate limiting. Such observation explains the much lower selectivity of NO_2^- on Cu/Ni electrode than the metallic Cu foam electrode. Notably, K_d on both Cu/Ni and Cu electrodes decreased significantly with increasing the negative potential, indicating that the selectivity of N_2 (k_5) was affected by the electrode potential. One can rationalize more NH_4^+ being reduced from N by hydrogen radicals accumulated onto the

Table 4
Effects of electrode material characteristics on electrochemical nitrate reduction.

Material factors	Electrodes	Methodology	Electrochemical conditions	Properties	Ref.
Morphology	SnPd/SS	Multi-step of electrodeposition using $SnCl_2$ and $PdCl_2$ electrolytes	112 mg/L NO_3^--N; 0.1 M $HClO_4$; pH 1.5 at 40 mA/cm^2	Ratio of Sn/Pd = 4; 80% nitrogen yield	[39]
	Sn/Pd	Electroless deposition on Pd metal in 0.12 mM $SnCl_2$ + 0.1 M $HClO_4$ solution for 2–20 min	0.01 M $NaNO_3$; 0.1 M $HClO_4$ at −0.2 V vs. Ag/AgCl	80% of Sn coverage; 51.3% nitrogen yield	[40]
	Cu	High-energy ball milling at different time	0.1 M $NaNO_3$; 1 M NaOH at −1.3 V vs. Hg/HgO	Milled copper with 73–74% nitrate reduction with 97% NH_3 selectivity	[41]
	Porous Cu/Pd	Electro-deposition at galvanostatic mode using 3 A/cm^2 using 0.5 M HCl and $CuCl_2$/$PdCl_2$	0.1 M $NaNO_3$; 1 M NaOH	Mostly produce NO_2^- and NH_3 over $Cu_{17}Pd_{83}$	[42]
	Nano-porous TiO_2/Ti	Two-step electrochemical anodization of nano Ti electrode (NTE)	100 mg/L NO_3^--N; 0.5 g/L Na_2SO_4 at 50 mA/cm^2	Current efficiency: ENTE (0.36) > NTE (0.25) > Ti metal (0.15)	[43]
	Ni/TiO_2/Ti	Ni deposition over anodized Ti using phosphinate as reducing agent	50 mg/L NO_3^--N; 0.5 g/L Na_2SO_4 at 30 mA/cm^2	Calcining temperature of Ni affects the efficiency of NO_3^- removal	[44]
	Co_3O_4/Ti	Sol-gel using 1 M $Co(NO_3)_2$ over Ti; annealed at 300–700 °C/2h	50 mg/L NO_3^--N; 0.1 M Na_2SO_4; pH 7 at 10 mA/cm^2	Co(II)/Co(III) couple mainly converted NO_3^- to NH_3	[45]
Crystal facet	Pt(1 0 0)/Pt (1 1 0)	Electro-deposition of Pt; 2 mM H_2PtCl_6 + 0.5 M H_2SO_4 at different windows of sweeping potential	10 mM KNO_3; 0.1 M $HClO_4$	NO_3^- on Pt(1 0 0) is reduced by fresh H_{ads} to finally produce ammonia	[46]
	Pt/Rh, Pt/Ir	Pulsed laser deposition at 3×10^{-8} bar	0.01 M NO_3^-; 0.5 M H_2SO_4	Pt(1 0 0) decreases the overpotential over $Pr_{42}Rh_{58}$ and $Pt_{25}Ir_{75}$	[47]
	Cu/Pt	Polishing of single crystal Pt and annealed at 1100 °C	0.02 M $NaNO_3$; 0.1 M $HClO_4$	The rate of nitrate electroreduction grows at low Cu coverages following Pt(2 1 0) < Pt(4 1 0) < Pt(6 1 0).	[48]
	Cu/Pt(1 1 1)	Polishing of single crystal Pt	5 mM $NaNO_3$;.1M $HClO_4$	Nitrate reduction improves by Cu monolayer; H on Pt inhibits the adsorption of nitrate	[49]
	Cu/Pt(1 0 0)	Electrodeposition of Pt on titanium foil in 10 mM HCl and 0.5 mM Na_2PtCl_6; underpotential deposition of Cu/Pt in 0.5 M H_2SO_4 + 2 mM $CuSO_4$.	0.1 M $NaNO_3$; 0.1 M NaOH at 0.15 V.	95% faradic efficiency of NO_3^-/NO_2^- conversion and 98% conversion selectivity on Cu adsorbed on 50% of Pt(1 0 0)	[50]
	Cu/Ni	Electroless Cu deposition on Ni foam using HCHO reductant	50 mg/L NO_3^--N, 0.1 M Na_2SO_4, pH 8.5	Nitrate efficiency (99% at 3 mA cm^{-2}) and selective conversion (55.6% at −0.6 V vs. Hg/HgO) improves with preference of Cu(1 1 1)	Present work

electrodes (Eqs. (14) and (15)) at higher overpotential with respect to HER.

Chemical reduction of nitrate ion has been performed directly using strong reducing agents, such as Ti^{2+}/Ti^{3+} over Ti electrode [11] and H_2 over SnPd catalysts [37,38]. Generation of secondary pollutants and regeneration of spent catalysts are two process challenges. Furthermore, direct nitrate reduction over specific electrodes without the addition of reducing agents could be eco-friendlier. However, interfacial activity between adsorbed nitrate and cathode is strongly influenced by the catalyst properties. Table 4 summaries the effect of electrode material characteristics relevant to improving the efficiency of nitrate reduction. Generally, the electrode characteristics pertinent to nitrate reduction efficiency can be divided into two major categories: (1) morphology, including surface roughness, particle size, crystal phase and porosity, and (2) crystal facet. The size reduction of Sn and Cu crystallites through multi-step deposition [39,40] and ball milling [41] resulted in high micro-surface area and roughness, which promoted the catalytic response of nitrate. Additionally, Pd metal is known to drastically enhance N_2 yield from NO_3^- reduction by favoring the capture of H_{ads} that is incorporated in CuPd and SnPd alloys [39,42]. Some transition metal oxides (TiO_2/Ti, Ni/TiO_2/Ti, Co_3O_4/Ti) exhibit significant nitrate adsorption and efficient electron transfer to nitrate simultaneously. Although Ti support leads to low selectivity of N_2, chlorine generation by anodic oxidation of Cl^- aids to the oxidation of ammonia and enhance nitrogen selectivity [43–45]. The manipulation of crystal facet is important to improve the rate and selectivity of nitrate reduction. The density and orientation of lattice atoms vary with crystal facet. Specific adsorption of nitrate over the Pt{1 0 0}, Pt{1 1 1}, and Pt {1 1 0} facets has been studied [46,47]. Nevertheless, the decorated Cu is rather critical to N_2 selectivity [48–50]. The present work revealed that the ratio of Cu{2 0 0}/Cu{1 1 1} controlled by the plating time was key to the performance of Cu/Ni electrode. The rate-determining NO_3^- adsorption step could be moderately improved to accelerate the reduction reaction when Cu{1 1 1} became a predominant and preferential facet.

4. Conclusion

The electrochemical behavior of nitrate reduction over Cu/Ni composite electrodes in Na_2SO_4 electrolyte was investigated. Surface characterization of the electrodes using XRD and SEM revealed that the crystal facet and grain shape of Cu nanoparticulates supported on the Ni foam substrate could be manipulated readily by the mode of electrodeless plating, specifically the reaction duration. According to cyclic voltammetry, the protonation of NO_3^- at potential around the onset of Cu(0)/Cu(I) redox couple (−0.6 V vs. Hg/HgO) proved the dependence of nitrate adsorption on the phase transition of surface cuprite oxide film. The transfer coefficient was maximized over the Cu/Ni/20-min electrode, for which the facet was preferentially oriented toward Cu {1 1 1}. Based on the peak currents from the voltammetry curves in the presence of KNO_3 at various concentrations and scan rates, the electron pathway was evaluated in the potential window of −0.6 V to −1.2 V: the first electron was indirectly mediated by $Cu^{(0)}$ at −0.6 V, and the subsequent reduction of the adsorbed NO_3^- to NO_2^- and $N_{(ads)}$, which then dimerized to N_2, whereas $N_{(ads)}$ was protonated to NH_4^+ by hydrogen radicals at a potential beyond HER, i.e., < -1.0 V on the Cu/Ni electrode. Because of morphological effect on nitrate reduction, Cu/Ni/10-min and Cu/Ni/20-min electrodes were highly effective (> 97% nitrate removal rate) compared to that of the Cu foam and Cu/Ni/60-min electrode. Results indicated that that Cu{1 1 1} played a significant role on nitrogen selectivity. At overpotential of $\geqslant -0.6$ V vs Hg/HgO, the selectivity of N_2 was 55.6%; however, at < -0.6 V vs Hg/HgO complete reduction of NO_3^- occurred and yielded NH_4^+ as major product.

Declaration of Competing Interest

The authors declare that they have no known competing financial interests or personal relationships that could have appeared to influence the work reported in this paper.

Acknowledgements

The authors would like to thank the Ministry of Science and Technology, Taiwan for financially supporting this research under Contract No. MOST 107-2221-E-110-001-MY3. Addition support was provided by US NSF IOA (1632899) to CPH.

Appendix A. Supplementary data

Supplementary data to this article can be found online at https://doi.org/10.1016/j.cej.2019.123157.

References

[1] P. Kuang, K. Natsui, Y. Einaga, Comparison of performance between boron-doped diamond and copper electrodes for selective nitrogen gas formation by the electrochemical reduction of nitrate, Chemosphere 210 (2018) 524–530.
[2] D. Çirmi, R. Aydın, F. Köleli, The electrochemical reduction of nitrate ion on polypyrrole coated copper electrode, J. Electroanal. Chem. 736 (2015) 101–106.
[3] E. Pérez-Gallent, M.C. Figueiredo, I. Katsounaros, M.T.M. Koper, Electrocatalytic reduction of nitrate on copper single crystals in acidic and alkaline solutions, Electrochim. Acta 227 (2017) 77–84.
[4] P. Singh, M.K. Singh, Y.R. Beg, G.R. Nishad, A review on spectroscopic methods for determination of nitrite and nitrate in environmental samples, Talanta 191 (2019) 364–381.
[5] World Health Organization, 2004. Rolling Revision of the WHO Guidelines for Drinking-waters Quality, Nitrates and Nitrites in Drinking-waters.
[6] S. Tyagi, D. Rawtani, N. Khatri, M. Tharmavaram, Strategies for nitrate removal from aqueous environment using nanotechnology: a review, J. Water Proc. Eng. 21 (2018) 84–95.
[7] Z. Zhang, Y. Han, C. Xu, W. Ma, H. Han, M. Zheng, H. Zhu, W. Ma, Microbial nitrate removal in biologically enhanced treated coal gasification wastewater of low COD to nitrate ratio by coupling biological denitrification with iron and carbon microelectrolysis, Biores. Technol. 262 (2018) 65–73.
[8] Q. Wang, W. Wang, B. Yan, W. Shi, F. Cui, C. Wang, Well-dispersed Pd-Cu bimetals in TiO_2 nanofiber matrix with enhanced activity and selectivity for nitrate catalytic reduction, Chem. Eng. J. 326 (2017) 182–191.
[9] J. Martínez, A. Ortiz, I. Ortiz, State-of-the-art and perspectives of the catalytic and electrocatalytic reduction of aqueous nitrates, Appl. Catal. B Environ. 207 (2017) 42–59.
[10] D. Cecconet, S. Zou, A.G. Capodaglio, Z. He, Evaluation of energy consumption of treating nitrate-contaminated groundwater by bioelectrochemical systems, Sci. Total Environ. 636 (2018) 881–890.
[11] F. Yao, Q. Yang, Y. Zhong, X. Shu, F. Chen, J. Sun, Y. Ma, Z. Fu, D. Wang, X. Li, Indirect electrochemical reduction of nitrate in water using zero-valent titanium anode: factors, kinetics, and mechanism, Water Res. 157 (2019) 191–200.
[12] W. Duan, G. Li, Z. Lei, T. Zhu, Y. Xue, C. Wei, C. Feng, Highly active and durable carbon electrocatalyst for nitrate reduction reaction, Water Res. 161 (2019) 126–135.
[13] J.F. Su, I. Ruzybayev, I. Shah, C.P. Huang, The electrochemical reduction of nitrate over micro-architectured metal electrodes with stainless steel scaffold, Appl. Catal. B Environ. 180 (2016) 199–209.
[14] M.R. Ehrenburg, A.I. Danilov, I.G. Botryakova, E.B. Molodkina, A.V. Rudnev, Electroreduction of nitrate anions on cubic and polyoriented platinum nanoparticles modified by copper adatoms, J. Electroanal. Chem. 802 (2017) 109–117.
[15] Y.J. Shih, Y.H. Huang, C.P. Huang, Oxidation of ammonia in dilute aqueous solutions over graphite-supported a- and b-lead dioxide electrodes (PbO_2@G), Electrochim. Acta 257 (2017) 444–454.
[16] Y.J. Shih, Y.H. Huang, C.P. Huang, Electrocatalytic ammonia oxidation over a nickel foam electrode: role of $Ni(OH)_2$(s)-NiOOH(s) nanocatalysts, Electrochim. Acta 263 (2018) 261–271.
[17] W. Root, N. Aguiló-Aguayo, T. Pham, T. Bechtold, Conductive layers through electroless deposition of copper on woven cellulose lyocell fabrics, Surf. Coat. Technol. 348 (2018) 13–21.
[18] S. Ghosh, Electroless copper deposition: f critical review, Thin Solid Films 669 (2019) 641–658.
[19] B.S. Gentle, P.S. Ellis, M.R. Grace, I.D. McKelvie, Flow analysis methods for the direct ultra-violet spectrophotometric measurement of nitrate and total nitrogen in freshwaters, Anal. Chim. Acta 704 (2011) 116–122.
[20] J.M. Lee, K.K. Jung, J.S. Ko, Growth mechanism and application of nanostructures fabricated by a copper sulfate solution containing boric acid, J. Electrochem. Soc. 163 (8) (2016) D407–D413.
[21] A.S. Myerson, Handbook of Industrial Crystallization, second ed., Butterworth-Heinemann, USA, 2002.

[22] Y. Su, H. Li, H. Ma, J. Robertson, A. Nathan, Controlling surface termination and facet orientation in Cu_2O nanoparticles for high photocatalytic activity: a combined experimental and density functional theory study, ACS Appl. Mater. Interfaces 9 (2017) 8100–8106.
[23] M.C. Biesinger, Advanced analysis of copper X-ray photoelectron spectra, Surf. Interface Anal. 49 (2017) 1325–1334.
[24] O.F. Lopes, H. Varela, Effect of annealing treatment on electrocatalytic properties of copper electrodes toward enhanced CO_2 reduction, ChemistrySelect 3 (2018) 9046–9055.
[25] B. Shruthi, B.J. Madhu, V.B. Raju, Influence of TiO_2 on the electrochemical performance of pasted typeβ-nickel hydroxide electrode in alkaline electrolyte, J. Energy Chem. 25 (2016) 41–48.
[26] G.E. Badea, Electrocatalytic reduction of nitrate on copper electrode in alkaline solution, Electrochim. Acta 54 (2009) 996–1001.
[27] D.W. Hwang, S. Lee, M. Seo, T.D. Chung, Recent advances in electrochemical non-enzymatic glucose sensors – A review, Anal. Chim. Acta 1033 (2018) 1–34.
[28] D. Reyter, D. Bélanger, L. Roue, Study of the electroreduction of nitrate on copper in alkaline solution, Electrochim. Acta 53 (2008) 5977–5984.
[29] N. Aouina, H. Cachet, C. Debiemme-chouvy, T.T.M. Tran, Insight into the electroreduction of nitrate ions at a copper electrode, in neutral solution, after determination of their diffusion coefficient by electrochemical impedance spectroscopy, Electrochim. Acta 55 (2010) 7341–7345.
[30] G.B. Darband, M. Aliofkhazraei, A.S. Rouhaghdam, Nickel nanocones as efficient and stable catalyst for electrochemical hydrogen evolution reaction, Internat. J. Hydrogen Energy 42 (2017) 14560–14565.
[31] S. Jung, S. Bae, W. Lee, Development of Pd − Cu/Hematite catalyst for selective nitrate reduction, Environ. Sci. Technol. 48 (2014) 9651–9658.
[32] S. Jung, A.N. Karaiskakis, E.J. Biddinger, Enhanced activity for electrochemical hydrogenation and hydrogenolysis of furfural to biofuel using electrodeposited Cu catalysts, Catal. Today 323 (2019) 26–34.
[33] D. Le, S. Stolbov, T.S. Rahman, Reactivity of the $Cu_2O(100)$ surface: insights from first principles calculations, Surf. Sci. 603 (2009) 1637–1645.
[34] Y. Shang, L. Cuo, Facet-controlled synthesis strategy of Cu_2O-based crystals for catalysis and sensing, Adv. Sci. 2 (2015) 1500140.
[35] A. Soon, M. Todorova, B. Delley, C. Stampf, Thermodynamic stability and structure of copper oxide surfaces: a first-principles investigation, Phys. Rev. B 75 (2007) 125420.
[36] Y. Zhang, B. Deng, T. Zhang, D. Gao, A.W. Xu, Shape effects of Cu_2O polyhedral microcrystals on photocatalytic activity, J. Phys. Chem. C 114 (2010) 5073–5079.
[37] S. Hamid, S. Bae, W. Lee, Novel bimetallic catalyst supported by red mud for enhanced nitrate reduction, Chem. Eng. J. 348 (2018) 877–887.
[38] J. Park, Y. Hwang, S. Bae, Nitrate reduction on surface of Pd/Sn catalysts supported by coal fly ash derived zeolites, J. Hazard. Mater. 374 (2019) 309–318.
[39] J.F. Su, W.F. Kuan, H. Liu, C.P. Huang, Mode of electrochemical deposition on the structure and morphology of bimetallic electrodes and its effect on nitrate reduction toward nitrogen selectivity, Appl. Catal. B-Environ. 257 (2019) 117909.
[40] M.M. Hossain, K. Nakata, T. Kawaguchi, K. Shimazu, Reduction of nitrate on electrochemically pre-reduced tin-modified palladium electrodes, J. Electroanal. Chem. 707 (2013) 59–65.
[41] D. Reyter, G. Chamoulaud, D. Bélanger, L. Roué, Electrocatalytic reduction of nitrate on copper electrodes prepared by high-energy ball milling, J. Electroanal. Chem. 596 (2006) 13–24.
[42] L. Mattarozzi, S. Cattarin, N. Comisso, R. Gerbasi, P. Guerriero, M. Musiani, E. Verlato, Electrodeposition of compact and porous Cu-Pd alloy layers and their application to nitrate reduction in alkali, Electrochim. Acta 230 (2017) 365–372.
[43] X. Ma, M. Li, F. Meng, L. Wang, C. Feng, N. Chen, X. Liu, Efficient nano titanium electrode via a two-step electrochemical anodization with reconstructed nanotubes: electrochemical activity and stability, Chemosphere 202 (2018) 177–183.
[44] F. Liu, K. Liu, M. Li, S. Hu, J. Li, X. L, X. Liu, Fabrication and characterization of a Ni-TNTA bimetallic nanoelectrode to electrochemically remove nitrate from groundwater, Chemosphere 223 (2019) 560–568.
[45] J. Gao, B. Jiang, C. Ni, Y. Qi, Y. Zhang, N. Oturan, M.A. Oturan, Non-precious Co_3O_4-TiO_2/Ti cathode based electrocatalytic nitrate reduction: preparation, performance and mechanism, Appl. Catal. B-Environ. 254 (2019) 391–402.
[46] Q. Wang, X. Zhao, J. Zhang, X. Zhang, Investigation of nitrate reduction on polycrystalline Pt nanoparticles with controlled crystal plane, J. Electroanal. Chem. 755 (2015) 210–214.
[47] M. Duca, N. Sacré, A. Wang, S. Garbarino, D. Guay, Enhanced electrocatalytic nitrate reduction by preferentially-oriented (100) PtRh and PtIr alloys: the hidden treasures of the 'miscibility gap', Appl. Catal. B-Environ. 221 (2018) 86–96.
[48] E.B. Molodkina, A.I. Danilov, M.R. Ehrenburg, J.M. Feliu, Regularities of nitrate electroreduction on Pt(S)[n(100)x(110)] stepped platinum single crystals modified by copper adatoms, Electrochim. Acta 278 (2018) 165–175.
[49] E.B. Molodkina, M.R. Ehrenburg, Y.M. Polukarov, A.I. Danilov, J. Souza-Garcia, J.M. Feliu, Electroreduction of nitrate ions on Pt(111) electrodes modified by copper adatoms, Electrochim. Acta 56 (2010) 154–165.
[50] C. Roy, J. Deschamps, M.H. Martin, E. Bertin, D. Reyter, S. Garbarino, L. Roué, D. Guay, Identification of Cu surface active sites for a complete nitrate-to-nitrite conversion with nanostructured catalysts, Appl. Catal. B-Environ. 187 (2016) 399–407.